RSC Advances

PAPER

View Article Online
View Journal | View Issue

Cite this: *RSC Adv.*, 2025, **15**, 2825

Synthesis, cytotoxicity, apoptosis-inducing activity and molecular docking studies of novel isatin–podophyllotoxin hybrids†

Ha Thanh Nguyen, [ab] Ket Tran Van,*[bd] Hai Pham-The, [c] Quang-Bao Le,[c] Giang Le-Nhat-Thuy, [ab] Tuyet Anh Dang Thi, [ab] Phuong Hoang Thi,[ab] Quynh Giang Nguyen Thi, [a] Anh Nguyen Tuan, [ab] Doan Vu Ngoc[d] and Tuyen Van Nguyen *[ab]

Podophyllotoxin, along with its numerous derivatives and related compounds, is well known for its broad-spectrum pharmacological activity, especially for anticancer potential. In this study, several isatin–podophyllotoxin hybrid compounds were successfully synthesized with good yields through microwave-prompted three-component reactions of 2-amino-1,4-naphthoquinone, various substituted isatins, and tetronic acid. Their cytotoxicity was assessed against four types of human cancer cell lines, HepG2 (hepatoma carcinoma), MCF7 (breast cancer), A549 (non-small lung cancer), and KB (epidermoid carcinoma), alongside nontumorigenic HEK-293 human embryonic kidney cells. Among 14 compounds screened, **7f** possessed the strongest cytotoxicity to KB and A549 cell lines, with IC_{50} values of 1.99 ± 0.22 and 0.90 ± 0.09 μM, respectively. Further studies revealed that product **7f** could arrest the cell cycle of A549 cells at S phase and induce apoptosis of A549 cells. This compound was examined for its binding ability against cyclin-dependent kinases (CDKs) and procaspase/caspase systems. The results indicated that **7f** exhibited significant interactions with the residues of the ATP binding sites of CDK2/cyclin A and CDK5/p25 and also activated procaspase 6 through stable zinc chelation. Additionally, physicochemical and pharmacokinetic properties related to drug-likeness, in parallel with toxicity, were computationally assessed to identify the main issues that need to be addressed in structural optimization. Taken together, compound **7f** was identified as a potent cytotoxic agent that could be considered for anticancer drug discovery and development.

Received 10th December 2024
Accepted 13th January 2025

DOI: 10.1039/d4ra08691k

rsc.li/rsc-advances

Introduction

Isatin (1*H*-indol-2,3-dione, **1**) is a natural alkaloid isolated from a diversity of plants such as *Boronia koniamboensis*, *Couroupita guianensis* Aubl, *Isatis tinctoria*, and *Melochia tomentosa* (Fig. 1).[1] In humans, it is found in the central nervous system (CNS), peripheral tissues, as well as body fluids.[2–4] As a versatile molecule with unique size and privileged electronic properties, isatin and its derivatives have presented vivid biological and pharmacological properties, including anti-microbial,[5] anti-cancer,[6] anti-convulsant,[7] anti-inflammatory,[8] anti-oxidant,[9] and anti-viral activities.[10] Isatin derivatives can act on a large number of biological targets, including tyrosine kinase, tubulin, phosphodiesterase 4B, histone deacetylase, and β-carbonic anhydrase, thereby triggering apoptosis.[11,12] Several studies have highlighted the potential of developing isatin-based compounds as promising anticancer agents.[13–15] Moreover, introducing various types of substituents at N-1, C-3 (C=O) and C in the benzene ring of isatin can modulate its biological properties.[16] Notably, a huge number of bioactive 3-substituted isatins as potent anticancer agents have been reported in the literature.[17–19] For example, sunitinib (**2**) and toceranib (**3**), known as isatin derivatives, are multi-receptor tyrosine kinase inhibitors with profound antitumor and antiangiogenic activities in clinical trials (Fig. 1).[20]

On the other hand, podophyllotoxin (**4**, Fig. 1), a naturally occurring cyclolignan, has been widely used as an anticancer agent due to its disruption of cell mitosis through the inhibition of tubulin polymerization; however, it failed clinical trials because of severe side effects and toxicity.[21,22] Recently, 4-aza-podophyllotoxins (**5**), known as podophyllotoxin derivatives, have attracted much interest owing to their outstanding

[a]*Institute of Chemistry, Vietnam Academy of Science and Technology (VAST), 18 Hoang Quoc Viet, Cau Giay, Hanoi, Vietnam. E-mail: ngvtuyen@hotmail.com; ngvtuyen@ich.vast.vn*

[b]*Graduate University of Science and Technology, VAST, 18 Hoang Quoc Viet, Cau Giay, Hanoi, Vietnam. E-mail: tranvket@gmail.com*

[c]*University of Science and Technology of Hanoi, VAST, 18 Hoang Quoc Viet, Cau Giay, Hanoi, Vietnam*

[d]*Military Technical Academy, 236 Hoang Quoc Viet, Bac Tu Liem, Hanoi, Vietnam*

† Electronic supplementary information (ESI) available. See DOI: https://doi.org/10.1039/d4ra08691k

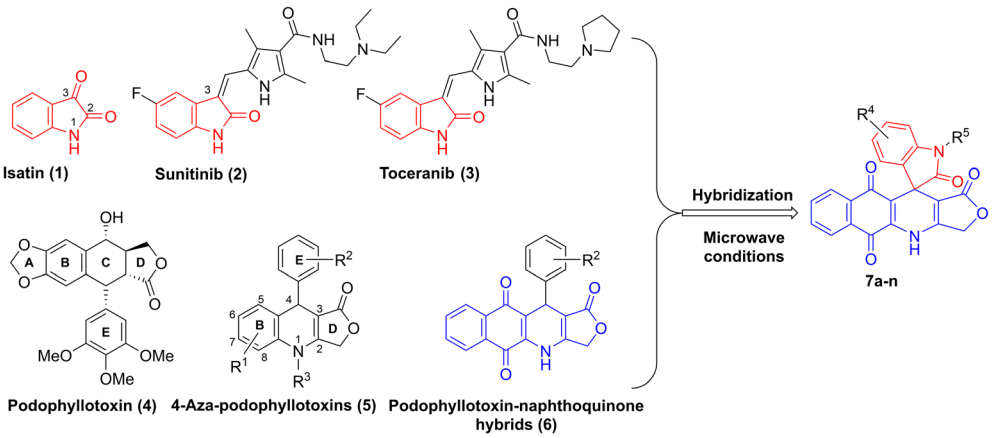

Fig. 1 Design of compounds **7a–n**.

biological activities, such as their antiproliferative effect on cancer cells, induction of apoptosis and cell cycle arrest in the G2/M phase, destabilization of microtubules, and vascular disruption effects.[23–26] Various aza-podophyllotoxins have exhibited activities comparable to podophyllotoxin (**4**).[27] By using multicomponent synthesis, which is a powerful and efficient method to prepare diverse and complex products in a single synthetic step with high selectivity, a wide variety of 4-aza-podophyllotoxin analogs with structural modifications in the B, E and D rings of the scaffold have been synthesized.[28–30] For instance, introducing 1,4-naphthoquinone to the B ring and different substituents in the E ring of 4-aza-podophyllotoxin, as well as keeping the intact γ-butylrolactone ring D, have furnished novel naphthoquinone–podophyllotoxin compounds **6** with strong cytotoxic effect on KB, HepG2 and SK-Lu-1 cancer cell lines (Fig. 1).[31,32]

The approach of merging two pharmacophores to enhance the biological and pharmacological potency of the resulting molecules is commonly employed in pharmaceutical and medicinal chemistry.[33] Therefore, we propose that incorporating isatins into a podophyllotoxin–naphthoquinone framework could synergize the molecular targets of both components, leading to the development of novel and promising anticancer agents. To the best of our knowledge, only one study has reported the synthesis of five isatin–podophyllotoxin hybrids *via* ultrasound-assisted four-component reactions,[34] and no research has been conducted on the biological activities of these hybrids. In light of the aforementioned findings and in a continuation of our endeavor with respect to the development of bioactive heterocyclic compounds,[35–38] we herein present a new convenient, efficient pathway to synthesize new isatin–podophyllotoxin hybrids **7a–n** (Fig. 1) as well as assessment of their cytotoxic activity against different cancer cell lines, namely hepatoma carcinoma (HepG2), breast (MCF7), non-small lung (A549) and epidermoid carcinoma (KB) cancer cell lines, using MTT (3-(4,5-dimethylthiazol-2-yl)-2,5-diphenyltetrazolium bromide) assay. Moreover, the most active molecule was further evaluated for its potential to induce apoptosis in the human A549 cancer cell line by conducting cell cycle analysis, apoptosis assay, and molecular docking analysis.

Results and discussion

Chemistry

In this study, novel substituted 3*H*-spiro[benzo[*g*]furo[3,4-*b*]quinoline-11,3′-indoline]-1,2′,5,10(4*H*)-tetraone derivatives (**7**) have been synthesized *via* microwave-assisted three-component reactions, in which various substituted isatins **10** (1 mmol) were applied to the mixture of 2-amino-1,4-naphthoquinone **8** (1 mmol) and tetronic acid **9** (1 mmol) in glacial acetic acid as solvent and in the presence of 20 mol% of *p*-toluenesulfonic acid (*p*-TsOH) as catalyst. The reactions were carried out under microwave irradiation (MW) at 120 °C for 20 min, resulting in the formation of substituted 3*H*-spiro[benzo[*g*]furo[3,4-*b*]quinoline-11,3′-indoline]-1,2′,5,10(4*H*)-tetraone derivatives in 70–85% yield (Scheme 1). Substituents attached to the isatin moiety were found to have no noticeable effect on the reaction's outcome. All obtained compounds were analysed using ^{1}H NMR, ^{13}C NMR, MS and IR techniques to confirm their molecular structure. Structure of product **7m** was reconfirmed using HSQC and HMBC.

A possible mechanistic explanation for the formation of products **7** is depicted in Scheme 2. Initially, intermediates **11** were built upon the Knoevenagel condensation between 2-amino-1,4-naphthoquinone (**8**) and substituted isatin **10**, followed by dehydration to afford intermediates **12**. Subsequent Michael addition of tetronic acid (**9**) to Michael acceptors **12** furnished intermediates **13**. An intramolecular cyclization followed by dehydration of intermediates **13** generated final products **7**.

Cytotoxicity of isatin–podophyllotoxin hybrids

The next objective of this study was to measure the *in vitro* cytotoxic activity of obtained products **7a–n** toward four types of human cancer cell lines (KB, HepG2, A549 and MCF7). For this objective, products **7** at different concentrations were firstly used to treat human cancer cells. Cytotoxic effects were measured using the MTT colorimetric assay, with ellipticine used as a ref. 39 and 40. The results revealed that all products **7a–n** exhibited moderate to strong inhibitory activity against the four tested cancer cell lines, with IC_{50} values ranging from 0.90

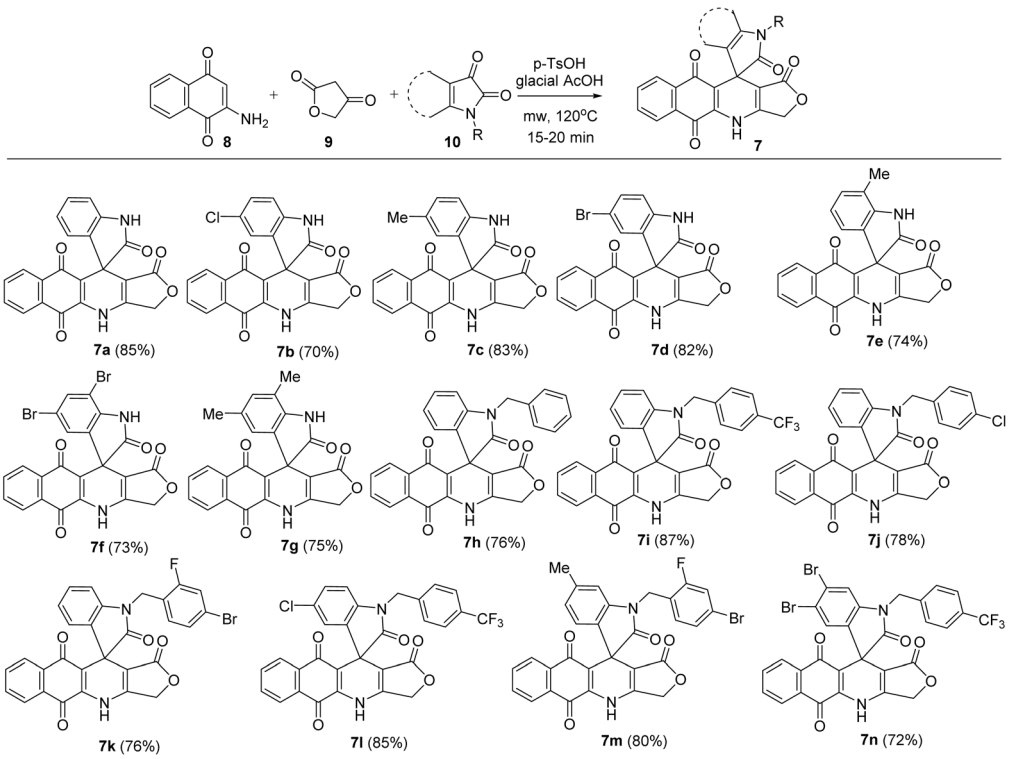

Scheme 1 Synthesis of isatin–podophyllotoxin hybrids **7a–n**.

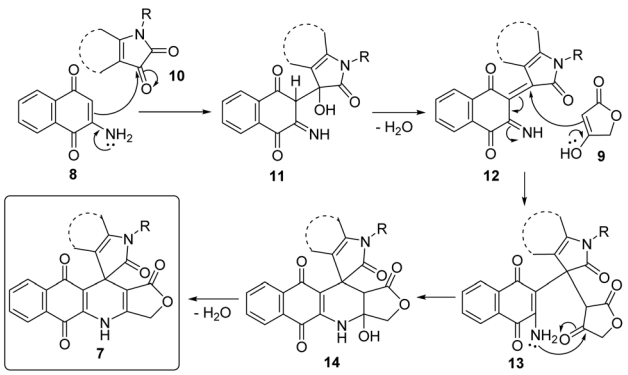

Scheme 2 The proposed reaction mechanism.

to 51.68 μM. Generally, products **7a–n** displayed lower cytotoxicity against HepG2 cells compared with that of ellipticine. Products **7a–d, g–h** exhibited potent growth inhibition values against A549 in the micromolar range (IC_{50} = 1.41–1.98 μM), close to that of the reference ellipticine ($IC_{50} = 1.34 \pm 0.08$ μM). The inhibitory activities against A549 cells of products **7f** ($IC_{50} = 0.90 \pm 0.09$ μM) and **7n** ($IC_{50} = 1.03 \pm 0.13$ μM) were better than that of ellipticine. In the case of MCF7 cells, products **7a** ($IC_{50} = 1.95 \pm 0.21$ μM), **7d** ($IC_{50} = 2.07 \pm 0.26$ μM), **7f** ($IC_{50} = 1.84 \pm 0.17$ μM), and **7n** ($IC_{50} = 2.11 \pm 0.24$ μM) showed similar or enhanced activity relative to ellipticine ($IC_{50} = 2.07 \pm 0.16$ μM). Interestingly, product **7f** possessed the strongest cytotoxicity to KB cells, with an IC_{50} value of 1.99 ± 0.22 μM. Moreover, the investigation on the toxicity of products **7a–n** on immortalized human embryonic kidney cells (Hek-293) revealed that products **7a–n** showed toxicity to Hek-293 (Table 1). Products **7f** and **7n** exhibited about 7-fold and 22-fold lower cytotoxicity against Hek-293 cells than to A549 cancer cell lines. Product **7n** exhibited about 11-fold lower cytotoxicity against Hek-293 cells than to MCF7 cancer cell lines. Based on the cytotoxicity data, it was found that the presence of bromo substituents in the benzene ring of isatin improved the inhibitory activity, as exemplified by products **7d**, **7f** and **7n**. Thus, the introduction of 4-bromo-2-fluorobenzyl substituent at N-1 of isatin produced products **7k** and **7m** with lower cytotoxic activity.

Among all products, product **7f** displayed the most potent activity against A549 cancer cell line, making it the selected compound for subsequent cell cycle analysis, apoptosis assay, and molecular docking studies.

Product 7f induced cell cycle S phase arrest in A549 cells

To determine whether the inhibition of cancer cell growth by product **7f** was associated with cell cycle arrest, A549 cells were treated with different concentrations of product **7f** (0.45 μM, 0.9 μM and 1.8 μM) for 24 hours. The distributions of cells in populations based on distinct phases including G0/G1 phase, S phase (synthesis), and G2/M phase (gap 2/mitosis) were analyzed by flow cytometry in cells stained with propidium iodide.[32,41] As shown in Fig. 2 and Table 2, treatment with product **7f** caused a significant rise of cell accumulation in S phase, accompanied by a decrease of cells in G0/G1 phase. These results suggested that the tested compound could dose-dependently arrest the cell cycle of A549 cells at S phase, thereby inhibiting cancer cell growth.

Table 1 Cytotoxicity of the products against KB, HepG2, MCF7, A549, and Hek-293 cell lines

		IC_{50}, μM				
Entry	Compound	KB	A549	HepG2	MCF7	Hek-293
1	**7a**	5.33 ± 0.62	1.98 ± 0.16	5.33 ± 0.62	**1.95 ± 0.21**	4.89 ± 0.44
2	**7b**	3.15 ± 0.21	1.41 ± 0.12	2.32 ± 0.31	4.20 ± 0.50	3.32 ± 0.33
3	**7c**	3.46 ± 0.33	1.91 ± 0.20	4.02 ± 0.45	4.17 ± 0.48	3.89 ± 0.40
4	**7d**	4.75 ± 0.41	1.62 ± 0.17	4.34 ± 0.41	**2.07 ± 0.26**	3.52 ± 0.37
5	**7e**	10.04 ± 0.93	2.28 ± 0.20	6.80 ± 0.63	18.83 ± 1.71	10.04 ± 1.08
6	**7f**	**1.99 ± 0.22**	**0.90 ± 0.09**	3.28 ± 0.39	**1.84 ± 0.17**	6.70 ± 0.57
7	**7g**	4.85 ± 0.41	1.67 ± 0.17	6.74 ± 0.68	2.62 ± 0.22	7.27 ± 0.78
8	**7h**	3.96 ± 0.34	1.71 ± 0.19	4.24 ± 0.38	3.73 ± 0.38	2.72 ± 0.19
9	**7i**	4.65 ± 0.44	7.37 ± 0.83	4.50 ± 0.48	3.72 ± 0.35	4.04 ± 0.42
10	**7j**	5.60 ± 0.49	6.54 ± 0.69	5.78 ± 0.61	4.09 ± 0.41	10.34 ± 1.06
11	**7k**	27.30 ± 2.15	14.00 ± 1.59	20.90 ± 2.36	15.09 ± 1.59	>28.00
12	**7l**	17.75 ± 1.68	5.93 ± 0.64	15.05 ± 1.70	13.40 ± 1.23	>27.73
13	**7m**	51.68 ± 1.78	13.28 ± 0.70	47.50 ± 2.15	19.85 ± 0.89	>64.96
14	**7n**	4.36 ± 0.40	**1.03 ± 0.13**	6.74 ± 0.73	**2.11 ± 0.24**	22.85 ± 2.20
15	Ellipticine	1.99 ± 0.16	1.34 ± 0.08	2.07 ± 0.12	2.07 ± 0.16	5.64 ± 0.32

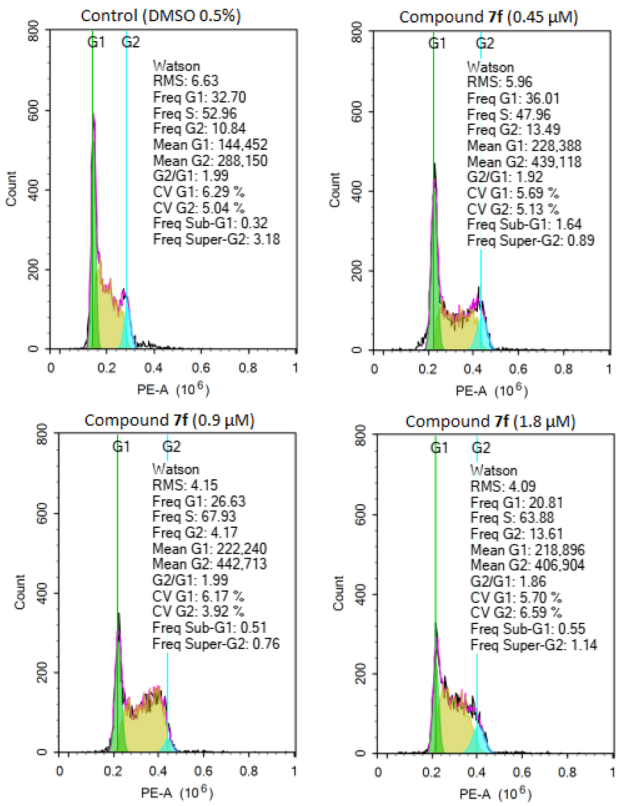

Fig. 2 Effect of compound **7f** on cell cycle distribution in A549 cells. Cells were treated with different concentrations of product **7f** (0.45 μM, 0.9 μM and 1.8 μM), DMSO 0.5% for 24 hours, stained with propidium iodide (PI) and analyzed for cell cycle using flow cytometry.

Product 7f induced apoptosis in A549 cells

Annexin-V FITC and PI flow cytometry assay for apoptosis. Fluorescent conjugates of annexin V can identify apoptotic cells by binding to phosphatidylserine (PS) exposed on the outer leaflet of their plasma membrane.[42,43] Thus, the apoptotic

Table 2 Percentage of cells by phases of product **7f** in A549 cell line

	Percentage of cells by phases (%)		
Sample	% G0/G1	% S	% G2/M
Control (DMSO 0.5%)	32.70	52.96	10.84
7f (0.45 μM)	36.01	47.96	13.49
7f (0.9 μM)	26.63	67.93	4.17
7f (1.8 μM)	20.81	63.88	13.61

effects of product **7f** were further assessed in the A549 cell line upon treatment by product **7f** for 48 hours at concentrations of 0.45 μM, 0.9 μM, and 1.8 μM using annexin V.[32,41] As illustrated in Fig. 3 and Table 3, treatment of cells with product **7f** at concentrations of 0.45 μM, 0.9 μM, and 1.8 μM resulted in a dose-dependent increase in apoptotic cell accumulation, from 2.48% (control) to 3.02%, 8.09%, and 19.4%, respectively. Therefore, the results indicated that product **7f** inhibited A549 cancer cell growth through inducing cellular apoptosis of A549 cells in a dose-dependent manner, particularly in the early apoptotic stage.

Molecular docking study

According to the design strategy and experimental assays, we found **7f** as a potential hit compound that could induce G1/S cell cycle arrest of cancer cells targeting apoptotic pathways, *e.g.*, procaspase/caspase activation and cyclin-dependent kinases (CDKs). It is worth noting that isatin–podophyllotoxin derivatives have not been explored for their binding interactions with CDKs. We therefore decided to perform docking simulations for **7f** and two CDK complexes, including CDK2/cyclin A and CDK5/p25, and one apoptosis effector, procaspase/caspase 6. CDK2 and CDK5 are the main regulators of the cell division cycle, in which CDK2 plays a significant role in the progression from G1 to S phase.[44] The association of

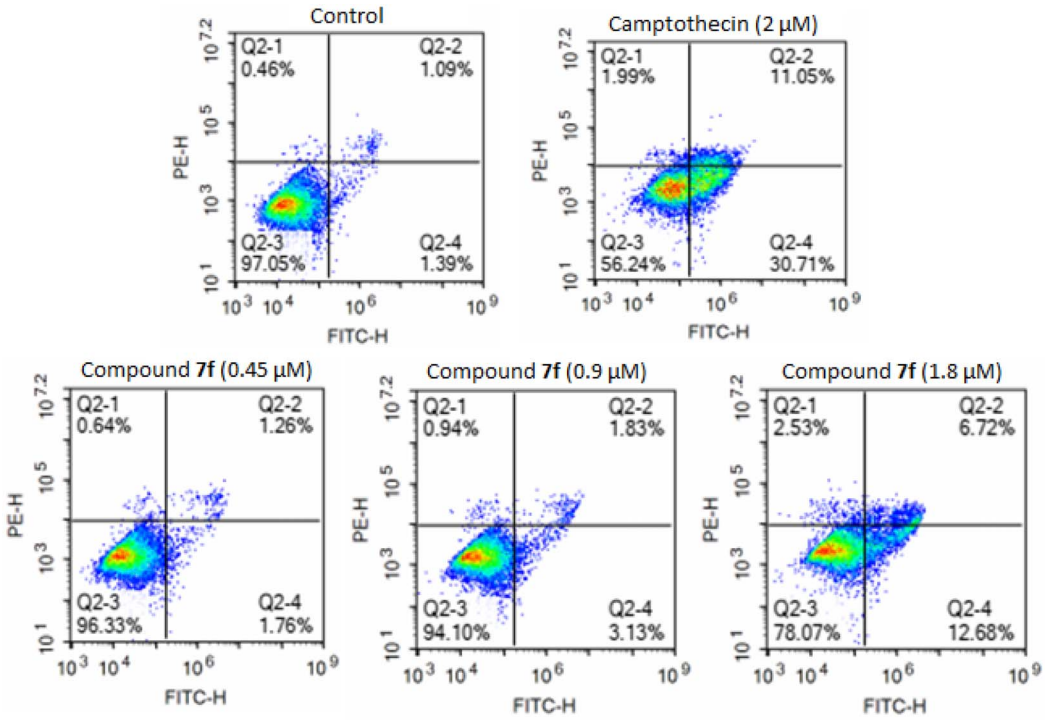

Fig. 3 Apoptosis population distribution of A549 cells treated with product **7f** using annexin-V/PI staining assay. Cells were treated with different concentrations of compound **7f** (0.45 μM, 0.9 μM and 1.8 μM), control, and camptothecin (2 μM) for 48 hours, stained with annexin-V/PI and analyzed for apoptosis using flow cytometry. The diverse cell stages were given as live (Q2-3), early apoptotic (Q2-4), late apoptotic (Q2-2), and necrotic cells (Q2-1).

Table 3 Percentage of apoptosis cells

Sample	% necrotic cells	% early apoptosis cells	% late apoptosis cells	% total apoptosis cells
Control	0.46	1.39	1.09	2.48
Camptothecin (2 μM)	1.99	30.71	11.05	41.76
7f (0.45 μM)	0.64	1.76	1.26	3.02
7f (0.9 μM)	0.94	3.13	1.83	8.09
7f (1.8 μM)	2.53	12.68	6.72	19.4

CDK2 with cyclin A (or cyclin E) and subsequent phosphorylation of the active loop are pivotal to make CDK2 fully active. CDK5 in turn exhibits regulatory function in a different manner. The binding with the activator p25 (or p35/p39) is the only step to activate this CDK without a phosphorylation process. The dysregulation of CDKs has been linked to various diseases, including cancer, severe neurodegenerative disorders, *etc.*[44]

As typical kinases, CDK2 and CDK5 have two globular domains, the N-terminal domain composed mostly of β-sheet and the C-terminal domain which is predominantly α-helix. According to the 3D structures published by Jeffrey *et al.*,[45] we identified that the catalytic cleft of CDK2/cyclin A includes a Gly rich loop (G-loop) which is located above the ATP binding pocket. The other α-helix, referred to as the PSTAIRE (Pro–Ser–Thr–Ala–Isoleu–Arg–Glu) helix, undergoes rearrangement and assists in repositioning the key residues within the active site (Fig. 4A). The T-loop, located at the interface of CDK2 and cyclin A, is more flexible than the G-loop and plays a role in phosphorylation. Therefore, we focused solely on the ATP binding site, as the compound is believed to disrupt the interaction between CDK2 and cyclin A. We initially redocked an ATP molecule and compared it with the co-crystal ligand to validate the protocol. The redocking result was suitable, as the redocked and co-crystal conformers showed a RMSD of 1.02 Å with a docking score of −35.84 kcal mol^{-1} and conserved important interactions in the active site. We then applied the validated docking method to estimate the binding modes of **7f** with CDK2/cyclin A. This compound bound to the hydrophobic secondary pocket, as Gleevec-like (type-II) kinase inhibitors normally act. As can be seen in Fig. 4C, isatin–podophyllotoxin derivative was found to be involved in numerous stacking interactions with Ala31, Val64, Leu134, and especially gatekeeper Phe80. In addition, H-bonds from NH and CO groups, as well as the 5,7-dibromoisatin moiety towards backbone O of

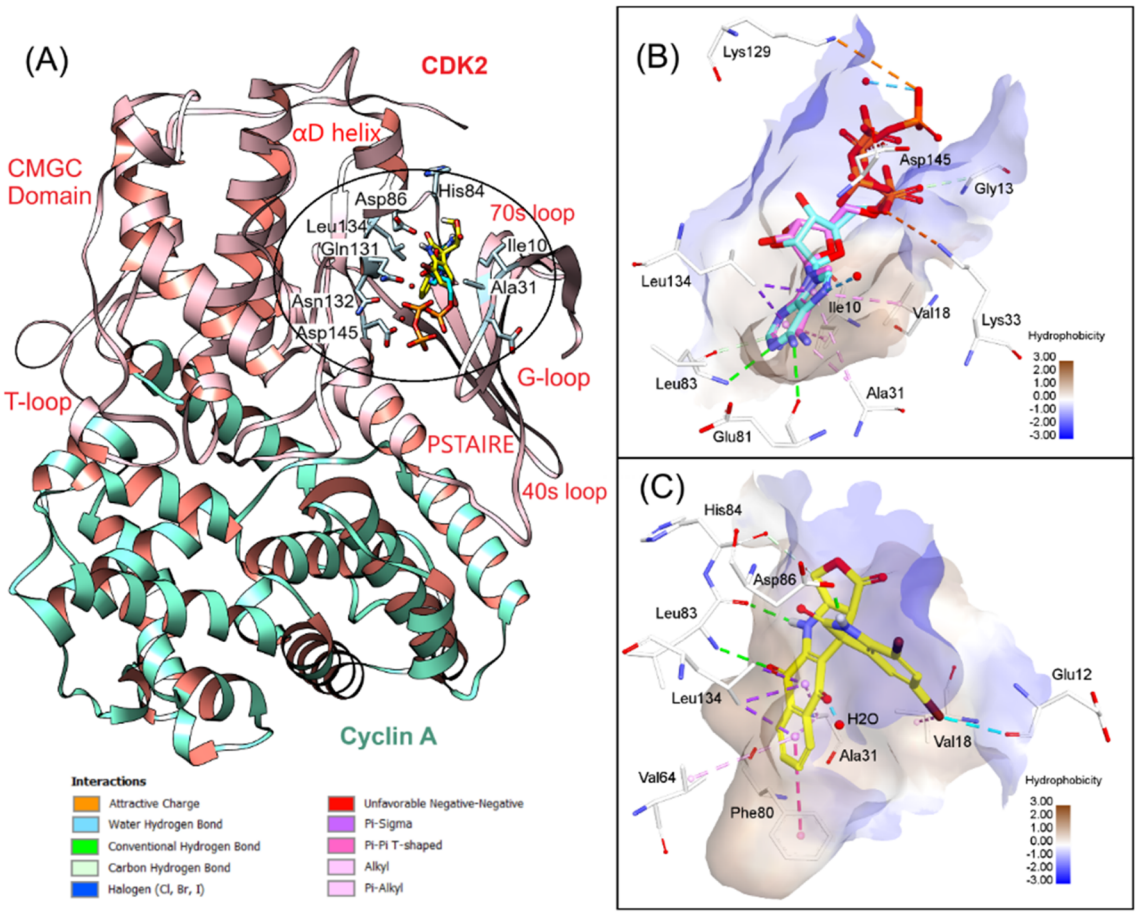

Fig. 4 3D visualization of (A) superposition of **7f** and ATP in CDK2/cyclin A (PDB ID 1FIN), (B) redocking results, and (C) **7f** interactions with the key residues at the ATP binding site.

Glu12, Leu83, and side chain O of Asp86, significantly stabilize the accommodation of **7f** at the ATP binding site of CDK2/cyclin A. A docking score of −27.35 kcal mol^{-1} was calculated for **7f**, which is slightly lower than that of the native ligand ATP.

We continued analyzing the structure of CDK5/p25 complex and performed docking simulations with the crystallographic structure reported by Mapelli *et al.*[46] Several studies have been conducted to understand the mechanism of activation of this complex.[47] In general, the structures of CDK5/p25 and CDK2/cyclin A are quite similar. Some dissimilarity was noted at the activation T-loop, but it does not affect the binding of roscovitine, a cell proliferation inhibitor, toward CDK5 N-terminal domain.[47] After redocking, roscovitine was found to be highly overlapped with the co-crystal ligand (RMSD = 0.791 Å), with a docking score of −23.14 kcal mol^{-1}. The key interactions, including H-bonds from the purine moiety with Glu81, Cys83, Asp86, as well as hydrophobic interactions between pyrazole and isopropyl rings with Leu10, Val18, Ala31 and Phe80, were conserved, suggesting the validity of the docking protocol for this system. We continued docking **7f** into the ATP binding site of CDK5/p25 and found that this compound even bound better to this pocket in comparison to roscovitine. Numerous H-bonds were observed between this compound and the hinge region residues such as Cys83, Gln85, Cys86, and Gln130. The extra stacking interactions formed between **7f** and the hydrophobic binding pocket were favorable for the binding of this derivative in the G-loop. The binding energy estimated by GBSA/MM-type scoring function was −26.02 kcal mol^{-1}, suggesting good affinity of **7f** to CDK5 (Fig. 5).

In the next step, the apoptosis induction activity of **7f** was examined by using docking simulations with a procaspase 6/caspase 6 in complex with PAC-1 (PDB ID 4FXO).[48] We have demonstrated previously that podophyllotoxin–naphthoquinone compounds can form stable bidentate chelation with inhibitory Zn ion, which is associated with their anticancer activity.[30,31] By running multiple sequence alignment (MSA) and phylogenetic analysis with seven caspase data using Clustal Omega (**https://www.ebi.ac.uk/jdispatcher/msa/clustalo**), we classified caspases 3, 6 and 7 as effectors of apoptosis (Fig. 6A). The catalytic activities of these effectors are blocked by Zn, which is coordinated with Lys36, Glu244, His287 and a water molecule.[31,48] By docking PAC-1 to the allosteric site of procaspase 6, we identified that this caspase activator could form stable chelation with inhibitory Zn ion and allow sequestering of Zn bound to procaspase.[49,50] We continued docking **7f** into the same pocket and revealed that this derivative also

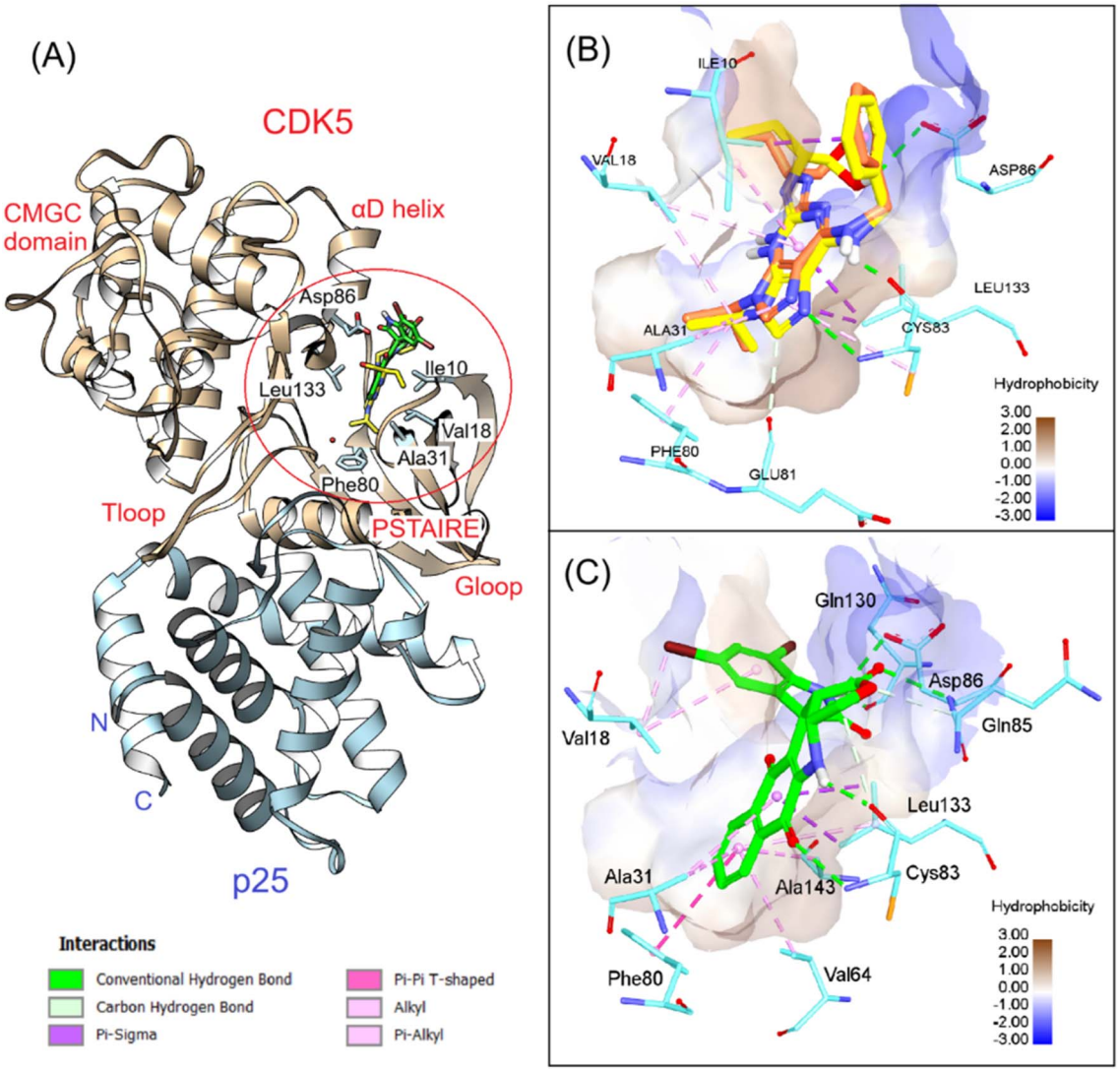

Fig. 5 3D visualization of (A) superposition of **7f** and roscovitine in CDK5/p25 (PDB ID 1UNL), (B) redocking results, and (C) **7f** interactions with the key residues at the ATP binding site.

formed bidentate chelation with Zn ion *via* the two C=O groups of 5,7-dibromoisatin and trans lactone fragments (Fig. 6B and C). These results indicated that the synthesized compound could activate procaspase in the same manner that PAC-1 did. However, there is a difference between the coordination geometries of **7f** and PAC-1 with Zn, and **7f** displayed lower docking scores (-19.10 kcal mol^{-1}) compared to PAC-1 (-23.81 kcal mol^{-1}).

Prediction of physicochemical and ADMET (absorption, distribution, metabolism, excretion, and toxicity) properties

It is desirable to examine the pharmacokinetic properties in parallel with biological activity of hit compound **7f**. We therefore applied several cheminformatics tools for the calculation of the physicochemical and ADMET properties of this compound.[51–56] The results are summarized in Fig. 7 and Table 4. Based on several drug-like rules, we identified that this compound accomplished the Lipinski and Pfizer rules but did not obey the GSK rule. Among the physicochemical properties calculated, lipophilicity (log *P*), solubility (log *S*), and number of rings (n_{Rig}) are out of drug-like ranges. In addition, it is provisionally classified as BCS class II, which may need some modifications to improve aqueous solubility.[52,55] Subsequently, the ADMET properties were evaluated, revealing that the primary concern would be the extensive metabolism by cytochrome P450. Compound **7f** was predicted to be a substrate for several first-pass metabolizing enzymes, including CYP3A4, CYP1A2, CYP2C9, and others (Table 4). It is therefore estimated that this compound would have low oral bioavailability. In terms of toxicity, **7f** did not show interaction with the human ether-à-go-go-related gene (hERG) channel, which is considered the main cause of cardiotoxicity. In addition, this compound showed low toxicity against skin, respiratory system and AMES except for the liver. Its oral acute toxicity in rats was determined to be low, with a lethal dose > 500 mg kg^{-1}.[51]

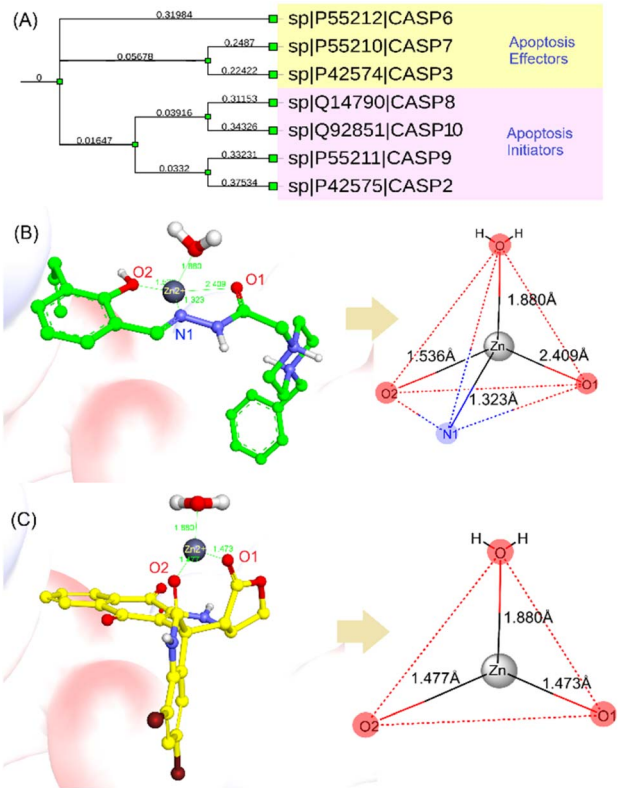

Fig. 6 (A) A dendrogram of selected caspases showing their role in apoptosis. Metal complex and geometries of PAC-1 of PAC-1 (B) and **7f** (C) against Zn ion extracted from procaspase-6 (PDB ID 4FXO).

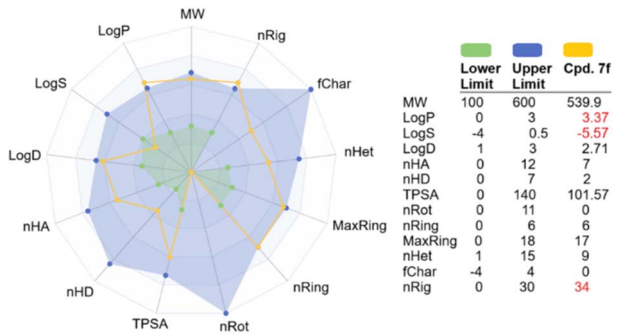

	Lower Limit	Upper Limit	Cpd. 7f
MW	100	600	539.9
LogP	0	3	3.37
LogS	-4	0.5	-5.57
LogD	1	3	2.71
nHA	0	12	7
nHD	0	7	2
TPSA	0	140	101.57
nRot	0	11	0
nRing	0	6	6
MaxRing	0	18	17
nHet	1	15	9
fChar	-4	4	0
nRig	0	30	34

Fig. 7 Predicted physicochemical properties of **7f** compared to optimal drug ranges. Abbreviations can be found in ADMETlab 3.0 web server (https://admetlab3.scbdd.com/).

Experimental

General considerations

All chemicals and solvents were purchased from Aldrich or Merck unless otherwise specified. Reactions were conducted in an Anton Paar Microwave Synthetic Reactor Monowave 400. To monitor reaction progress, thin layer chromatography (TLC) was performed using TLC silica gel 60 F_{254} visualized under UV light at 254 nm. Purification of the compounds was achieved through open silica gel column flash chromatography, employing Merck silica gel 60 (240–400 mesh) as the stationary phase. Melting points were determined using a Buchi Melting Point B-545 and were uncorrected. Infrared (IR) analysis was conducted with a PerkinElmer Spectrum Two spectrometer using KBr pellets. NMR spectra (^{1}H, ^{13}C) were recorded on a Bruker Avance III spectrometer (600 and 150 MHz) with tetramethylsilane used as the internal standard. HRMS was performed on an SCIEX X500 QTOF mass spectrometer.

General procedure for the synthesis of products 7a–n

A vial containing a mixture of 2-amino-1,4-naphthoquinone **8** (1 mmol), tetronic acid **9** (1 mmol), isatin derivative **10** (1 mmol), and *p*-TsOH (0.02 mmol) in glacial acetic acid (3 mL) was subjected to microwave irradiation (120 °C and 150 W). Following a reaction time of 15 to 20 minutes, the vial was cooled to room temperature, and 20 mL of water was added to the mixture. The product was extracted with dichloromethane (3 × 20 mL), washed with brine (3 × 10 mL), and dried using Na_2SO_4. The solvent was evaporated to yield crude product which was purified by column chromatography with a dichloromethane–ethyl acetate eluent (25 : 4, 20 : 1, v/v) to afford product **7**.

3*H*-Spiro[benzo[*g*]furo[3,4-*b*]quinoline-11,3′-indoline]-1,2′,5,10(4*H*)-tetraone (7a). Yield 327 mg (85%), red-brown solid, mp 356–357 °C. IR (KBr) ν_{max}/cm^{-1} 3133, 3081, 3032, 2840, 1756, 1708, 1663, 1617, 1592, 1498, 1473, 1394, 1335, 1302, 1265, 1202, 1180, 1143, 1082, 1020, 970, 789, 753, 723, 621. ^{1}H NMR (DMSO-d_6, 600 MHz) δ 10.90 (1H, s, NH), 10.51 (1H, s, NH), 8.08 (1H, dd, J = 6.6, 1.8 Hz, H-6), 7.86–7.80 (3H, m, H-7, H-8, H-9), 7.15 (1H, td, J = 7.2, 1.2 Hz, H-4′), 7.10 (1H, d, J = 7.2 Hz, H-5′), 6.83 (1H, td, J = 7.2, 1.2 Hz, H-6′), 6.81 (1H, d, J = 7.2 Hz, H-7′), 4.99 (1H, d, J = 16.8 Hz, H-3), 4.97 (1H, d, J = 16.8 Hz, H-3). ^{13}C NMR (DMSO-d_6, 150 MHz) δ 181.1 (C-10), 179.1 (C-5), 177.9 (C-2′), 169.2 (C-1), 156.1, 141.9, 140.7, 135.5, 135.1, 133.6, 131.5, 129.9, 128.4, 126.1, 125.9, 124.1, 121.3, 117.5, 108.8, 101.0, 66.1 (C-3), 48.0 (C-11). HR-ESI-MS: found m/z 385.0804 $[M + H]^+$ (calcd for $[C_{22}H_{13}N_2O_5]^+$: 385.0819) and m/z 407.0631 $[M + Na]^+$ (calcd for $[C_{22}H_{12}N_2NaO_5]^+$: 407.0639).

5′-Chloro-3*H*-spiro[benzo[*g*]furo[3,4-*b*]quinoline-11,3′-indoline]-1,2′,5,10(4*H*)-tetraone (7b). Yield 293 mg (70%), red-brown solid, mp 365–366 °C. IR (KBr) ν_{max}/cm^{-1} 3153, 3115, 3048, 2859, 1757, 1713, 1686, 1665, 1638, 1619, 1590, 1496, 1475, 1395, 1337, 1302, 1266, 1198, 1085, 1041, 1021, 1007, 973, 812, 725, 642, 554. ^{1}H NMR (DMSO-d_6, 600 MHz) δ 10.96 (1H, s, NH), 10.67 (1H, s, NH), 8.10–8.07 (1H, m, H-6), 7.86–7.81 (3H, m, H-7, H-8, H-9), 7.24 (1H, d, J = 2.4 Hz, H-4′), 7.20 (1H, dd, J = 8.4, 2.4 Hz, H-6′), 6.83 (1H, d, J = 7.8 Hz, H-7′), 5.00 (2H, s, H-3). ^{13}C NMR (DMSO-d_6, 125 MHz) δ 181.4 (C-10), 179.1 (C-5), 177.8 (C-2′), 169.3 (C-1), 156.6, 141.0, 140.9, 137.1, 135.2, 133.7, 131.5, 130.0, 128.3, 126.2, 126.0, 125.4, 124.5, 116.9, 110.3, 100.5, 66.3 (C-3), 48.3 (C-11). HR-ESI-MS: found m/z 419.0434 $[M + H]^+$ (calcd for $[C_{22}H_{12}ClN_2O_5]^+$: 419.0429).

5′-Methyl-3*H*-spiro[benzo[*g*]furo[3,4-*b*]quinoline-11,3′-indoline]-1,2′,5,10(4*H*)-tetraone (7c). Yield 331 mg (83%), red solid, mp 361–362 °C. IR (KBr) ν_{max}/cm^{-1} 3328, 3031, 2915, 2862, 2796, 2735, 1753, 1730, 1669, 1631, 1588, 1494, 1396, 1336, 1310, 1266, 1203, 1072, 1042, 1020, 999, 820, 722, 691, 601. ^{1}H NMR (DMSO-d_6, 600 MHz) δ 10.89 (1H, s, NH), 10.41 (1H, s,

Table 4 Summary of ADMET properties of **7f**

Property	Predicted value	Unit
Absorption		
Caco2 permeability	−4.788	log P_{app} in 10^{-6} cm s^{-1}
P-glycoprotein substrate	Yes	Categorical (yes/no)
Human intestinal absorption (HIA)	>30	% absorbed
Bioavailability (*F*)	<20	% oral bioavailable
Distribution		
Human distribution volume (VDss)	4.236	log L kg^{-1}
Fraction unbound	2.1	F_u%
Blood–brain barrier (BBB) permeability	Yes	Categorical (yes/no)
Metabolism		
CYP2D6 substrate	No	Categorical (yes/no)
CYP3A4 substrate	Yes	Categorical (yes/no)
CYP1A2 substrate	Yes	Categorical (yes/no)
CYP2C19 substrate	Yes	Categorical (yes/no)
CYP2C9 substrate	Yes	Categorical (yes/no)
Excretion		
Total clearance	1.935	CL_{plasma}, mL min^{-1} kg^{-1}
T1/2	1.105	Hour
Toxicity		
AMES toxicity	No	Categorical (yes/no)
hERG inhibitor	No	Categorical (yes/no)
Hepatotoxicity	Yes	Categorical (yes/no)
Skin sensitization	No	Categorical (yes/no)
Rat oral acute toxicity	0.832	Low-toxicity, >500 mg kg^{-1}

NH), 8.07 (1H, dd, $J = 7.8$, 1.8 Hz, H-6), 7.85–7.80 (3H, m, H-7, H-8, H-9), 6.95 (2H, d, $J = 10.8$ Hz, H-4′, H-6′), 6.70 (1H, d, $J = 7.8$ Hz, H-7′), 4.99 (2H, s, H-3), 2.14 (3H, s, CH_3). ^{13}C NMR (DMSO-d_6, 150 MHz) δ 181.1 (C-10), 179.1 (C-5), 177.9 (C-2′), 169.2 (C-1), 156.1, 140.6, 139.4, 135.6, 135.1, 133.6, 131.5, 130.2, 129.9, 128.6, 126.1, 125.9, 124.8, 117.6, 108.6, 101.1, 66.0 (C-3), 48.1 (C-11), 20.5 (CH_3). HR-ESI-MS: found *m*/*z* 399.0964 $[M + H]^+$ (calcd for $[C_{23}H_{15}N_2O_5]^+$: 399.0976) and *m*/*z* 421.0788 $[M + Na]^+$ (calcd for $[C_{23}H_{14}N_2NaO_5]^+$: 421.0795).

5′-Bromo-3*H*-spiro[benzo[*g*]furo[3,4-*b*]quinoline-11,3′-indoline]-1,2′,5,10(4*H*)-tetraone (7d). Yield 379 mg (82%), red solid, mp (decomp.) 310–311 °C. IR (KBr) ν_{max}/cm^{-1} 3112, 3045, 2976, 2856, 2255, 1757, 1713, 1663, 1637, 1616, 1590, 1495, 1475, 1395, 1337, 1303, 1265, 1197, 1085, 1022, 1004, 809, 724, 640, 535. ^{1}H NMR (DMSO-d_6, 600 MHz) δ 10.96 (1H, s, NH), 10.68 (1H, s, NH), 8.07 (1H, dd, $J = 7.8$, 1.8 Hz, H-6), 7.87–7.81 (3H, m, H-7, H-8, H-9), 7.36 (1H, d, $J = 1.8$ Hz, H-4′), 7.33 (1H, dd, $J = 8.4$, 1.8 Hz, H-6′), 6.79 (1H, d, $J = 8.4$ Hz, H-7′), 5.00 (2H, s, H-3). ^{13}C NMR (DMSO-d_6, 150 MHz) δ 181.3 (C-10), 179.0 (C-5), 177.6 (C-2′), 169.2 (C-3), 156.5, 141.3, 141.0, 137.5, 135.1, 133.6, 131.5, 131.1, 130.0, 127.1, 126.1, 125.9, 116.8, 113.0, 110.7, 100.5, 66.2 (C-3), 48.2 (C-11). HR-ESI-MS: found *m*/*z* 462.9936 and 464.9912 $[M + H]^+$ (calcd for $[C_{22}H_{12}BrN_2O_5]^+$: 462.9924 and 464.9904) and *m*/*z* 484.9749 and 486.9726 $[M + Na]^+$ (calcd for $[C_{22}H_{11}BrN_2NaO_5]^+$: 484.9744 and 486.9724).

7′-Methyl-3*H*-spiro[benzo[*g*]furo[3,4-*b*]quinoline-11,3′-indoline]-1,2′,5,10(4*H*)-tetraone (7e). Yield 295 mg (74%), brown-orange solid, mp (decomp.) 367–368 °C. IR (KBr) ν_{max}/cm^{-1} 3153, 2854, 1721, 1667, 1625, 1595, 1490, 1396, 1331, 1296, 1269, 1214, 1084, 1041, 1028, 839, 767, 721, 569. ^{1}H NMR (DMSO-d_6, 600 MHz) δ 10.89 (1H, s, NH), 10.55 (1H, s, NH), 8.08–8.06 (1H, m, H-6), 7.86–7.80 (3H, m, H-7, H-8, H-9), 6.97 (1H, d, $J = 7.2$ Hz, H-4′), 6.92 (1H, d, $J = 7.2$ Hz, H-6′), 6.75 (1H, t, $J = 7.2$ Hz, H-5′), 4.99 (1H, dd, $J = 16.8$ Hz, H-3), 4.97 (1H, d, $J = 16.8$ Hz, H-3), 2.27 (3H, s, CH_3). ^{13}C NMR (DMSO-d_6, 125 MHz) δ 181.1 (C-10), 179.1 (C-5), 178.4 (C-2′), 169.2 (C-1), 156.0, 140.5, 140.4, 135.2, 135.1, 133.6, 131.5, 129.9, 129.8, 126.1, 125.9, 121.6, 121.3, 117.8, 117.6, 101.1, 66.0 (C-3), 48.3 (C-11), 16.4 (CH_3). HR-ESI-MS: found *m*/*z* 399.0967 $[M + H]^+$ (calcd for $[C_{23}H_{15}N_2O_5]^+$: 399.0976) and *m*/*z* 421.0780 $[M + Na]^+$ (calcd for $[C_{23}H_{14}N_2NaO_5]^+$: 421.0795).

5′,7′-Dibromo-3*H*-spiro[benzo[*g*]furo[3,4-*b*]quinoline-11,3′-indoline]-1,2′,5,10(4*H*)-tetraone (7f). Yield 396 mg (73%), orange solid, mp (decomp.) 364–365 °C. IR (KBr) ν_{max}/cm^{-1} 3164, 3084, 2860, 1724, 1667, 1645, 1593, 1501, 1463, 1400, 1336, 1299, 1183, 1078, 1043, 1022, 1003, 979, 803, 725, 560. ^{1}H NMR (DMSO-d_6, 600 MHz) δ 11.05 (1H, s, NH), 11.03 (1H, s, NH), 8.09 (1H, dd, $J = 6.6$, 1.8 Hz, H-6), 7.86–7.82 (3H, m, H-7, H-8, H-9), 7.59 (1H, d, $J = 1.8$ Hz, H-6′), 7.42 (1H, d, $J = 1.8$ Hz, H-4′), 5.04 (1H, dd, $J = 16.8$ Hz, H-3), 5.02 (1H, d, $J = 16.8$ Hz, H-3). ^{13}C NMR (DMSO-d_6, 125 MHz) δ 181.4 (C-10), 179.0 (C-5), 177.6 (C-2′), 169.3 (C-1), 156.8, 141.2, 141.1, 138.2, 135.2, 133.8, 133.1, 131.4, 130.1, 126.5, 126.2, 126.1, 116.6, 113.6, 102.1, 100.3, 66.4 (C-3), 49.4 (C-11). HR-ESI-MS: found *m*/*z* 542.9003 and 540.9027

and 544.9012 $[M + H]^+$ (calcd for $[C_{22}H_{11}Br_2N_2O_5]^+$: 542.9009 and 540.9030 and 544.8989) and *m*/*z* 564.8824 and 562.8872 and 566.8793 $[M + Na]^+$ (calcd for $[C_{22}H_{10}Br_2N_2NaO_5]^+$: 564.8829 and 562.8849 and 566.8809).

4′,6′-Dimethyl-3*H*-spiro[benzo[*g*]furo[3,4-*b*]quinoline-11,3′-indoline]-1,2′,5,10(4*H*)-tetraone (7g). Yield 309 mg (75%), orange-red solid, mp 372–373 °C. IR (KBr) ν_{max}/cm^{-1} 3353, 3183, 1749, 1725, 1666, 1592, 1488, 1396, 1333, 1298, 1269, 1183, 1075, 1040, 1020, 752, 725. ^{1}H NMR (DMSO-d_6, 600 MHz) δ 10.87 (1H, s, NH), 10.45 (1H, s, NH), 8.08 (1H, m, H-6), 7.84–7.80 (3H, m, H-7, H-8, H-9), 6.76 (2H, d, J = 17.4 Hz, H-4′, H-6′), 4.98 (2H, s, H-3), 2.23 (3H, s, CH_3-5′), 2.11 (3H, s, CH_3-7′). ^{13}C NMR (DMSO-d_6, 150 MHz) δ 181.1 (C-10), 179.1 (C-5), 178.3 (C-2′), 169.2 (C-1), 155.9, 140.5, 138.0, 135.3, 135.1, 133.5, 131.5, 130.3, 130.1, 129.9, 126.1, 125.9, 122.2, 117.8, 117.5, 101.2, 66.0 (C-3), 48.3 (C-11), 20.4 (CH_3-5′), 16.3 (CH_3-7′). HR-ESI-MS: found *m*/*z* 413.1131 $[M + H]^+$ (calcd for $[C_{24}H_{17}N_2O_5]^+$: 413.1132) and *m*/*z* 435.0948 $[M + Na]^+$ (calcd for $[C_{24}H_{16}N_2NaO_5]^+$: 435.0952).

1′-Benzyl-3*H*-spiro[benzo[*g*]furo[3,4-*b*]quinoline-11,3′-indoline]-1,2′,5,10(4*H*)-tetraone (7h). Yield 361 mg (76%), red-brown solid, mp (decomp.) 320–321 °C. IR (KBr) ν_{max}/cm^{-1} 3431, 3061, 1752, 1712, 1667, 1608, 1497, 1333, 1300, 1267, 1181, 1075, 1041, 1018, 961, 747, 721. ^{1}H NMR (DMSO-d_6, 600 MHz) δ 11.03 (1H, s, NH), 8.11–8.08 (1H, m, H-6), 7.85–7.81 (3H, m, H-7, H-8, H-9), 7.63 (2H, d, J = 7.2 Hz), 7.36 (2H, t, J = 7.2 Hz), 7.29 (1H, t, J = 7.2 Hz), 7.21 (1H, dd, J = 7.8, 0.6 Hz), 7.14 (1H, td, J = 7.8, 1.2 Hz), 6.91 (1H, d, J = 7.8, 1.2 Hz), 6.69 (1H, d, J = 7.8 Hz), 5.05 (1H, d, J = 16.2 Hz), 5.04 (2H, d, J = 3.6 Hz), 4.94 (1H, d, J = 16.2 Hz). ^{13}C NMR (DMSO-d_6, 125 MHz) δ 181.2 (C-10), 179.0 (C-5), 176.7 (C-2′), 169.2 (C-1), 156.5, 142.5, 140.8, 136.3, 135.1, 134.5, 133.6, 131.4, 129.9, 128.5, 128.3 (2C), 127.2 (2C), 127.0, 126.2, 126.0, 124.1, 122.2, 117.2, 108.4, 100.8, 66.2 (C-3), 47.7 (C-11), 43.7 (C-7″). HR-ESI-MS: found *m*/*z* 475.1281 $[M + H]^+$ (calcd for $[C_{29}H_{19}N_2O_5]^+$: 475.1289) and *m*/*z* 497.1094 $[M + Na]^+$ (calcd for $[C_{29}H_{18}N_2NaO_5]^+$: 497.1108).

1′-(4-(Trifluoromethyl)benzyl)-3*H*-spiro[benzo[*g*]furo[3,4-*b*]quinoline-11,3′-indoline]-1,2′,5,10(4*H*)-tetraone (7i). Yield 472 mg (87%), orange-red solid, mp (decomp.) 335–336 °C. IR (KBr) ν_{max}/cm^{-1} 3314, 3066, 1763, 1708, 1671, 1611, 1505, 1421, 1371, 1323, 1300, 1268, 1163, 1124, 1067, 1015, 907, 803, 751, 726. ^{1}H NMR (DMSO-d_6, 600 MHz) δ 11.05 (1H, s, NH), 8.11–8.08 (1H, m, H-6), 7.86 (2H, d, J = 7.8 Hz), 7.85–7.82 (3H, m), 7.73 (2H, d, J = 7.8 Hz), 7.23 (1H, dd, J = 7.8, 1.2 Hz), 7.16 (1H, td, J = 7.8, 1.2 Hz), 6.93 (1H, td, J = 7.8, 1.2 Hz), 6.75 (1H, d, J = 7.8 Hz), 5.15 (1H, d, J = 16.8 Hz), 5.07 (1H, d, J = 16.8 Hz), 5.05 (2H, d, J = 3.6 Hz). ^{13}C NMR (DMSO-d_6, 125 MHz) δ 181.3 (C-10), 179.0 (C-5), 176.7 (C-2′), 169.4 (C-1), 156.6, 142.2, 141.4, 140.9, 135.2, 134.5, 133.7, 131.4, 130.0, 128.6, 128.0 (3C), 126.2, 126.1, 125.2 (2C, d, J = 3.8 Hz), 124.3 (1C, q, J = 271.3 Hz, CF_3), 124.3, 122.5, 117.1, 108.3, 100.8, 66.3 (C-3), 47.7 (C-11), 43.2 (C-7″). HR-ESI-MS: found *m*/*z* 543.1137 $[M + H]^+$ (calcd for $[C_{30}H_{18}F_3N_2O_5]^+$: 543.1162) and *m*/*z* 565.0952 $[M + Na]^+$ (calcd for $[C_{30}H_{17}F_3N_2NaO_5]^+$: 565.0982).

1′-(4-Chlorobenzyl)-3*H*-spiro[benzo[*g*]furo[3,4-*b*]quinoline-11,3′-indoline]-1,2′,5,10(4*H*)-tetraone (7j). Yield 397 mg (78%), orange-brown solid, mp (decomp.) 292–293 °C. IR (KBr) ν_{max}/cm^{-1} 3164, 3061, 1760, 1708, 1671, 1645, 1595, 1504, 1490, 1400, 1370, 1331, 1299, 1268, 1188, 1176, 1070, 1042, 1010, 907, 800, 748, 726, 572, 476. ^{1}H NMR (DMSO-d_6, 600 MHz) δ 11.04 (1H, s, NH), 8.11–8.07 (1H, m, H-6), 7.85–7.81 (3H, m, H-7, H-8, H-9), 7.65 (2H, d, J = 8.4 Hz), 7.42 (2H, dt, J = 8.4, 2.4 Hz), 7.21 (1H, d, J = 7.8, 1.2 Hz), 7.15 (1H, td, J = 7.8, 1.2 Hz), 6.91 (1H, td, J = 7.8, 1.2 Hz), 6.73 (1H, d, J = 7.8 Hz), 5.04 (1H, d, J = 16.2 Hz), 5.03 (2H, d, J = 3.6 Hz), 4.95 (1H, d, J = 16.2 Hz, H-7″). ^{13}C NMR (DMSO-d_6, 125 MHz) δ 181.3 (C-10), 179.0 (C-5), 176.7 (C-2′), 169.3 (C-1), 156.5, 142.3, 140.9, 135.4, 135.2, 134.5, 133.7, 131.8, 131.4, 130.0, 129.3 (2C), 128.6, 128.3 (2C), 126.2, 126.1, 124.2, 122.4, 117.1, 108.4, 100.8, 66.3 (C-3), 47.7 (C-11), 43.0 (C-7″). HR-ESI-MS: found *m*/*z* 509.0895 $[M + H]^+$ (calcd for $[C_{29}H_{18}ClN_2O_5]^+$: 509.0899) and *m*/*z* 531.0694 $[M + Na]^+$ (calcd for $[C_{29}H_{17}ClN_2NaO_5]^+$: 531.0719).

1′-(4-Bromo-2-fluorobenzyl)-3*H*-spiro[benzo[*g*]furo[3,4-*b*]quinoline-11,3′-indoline]-1,2′,5,10(4*H*)-tetraone (7k). Yield 434 mg (76%), orange solid, mp (decomp.) 350–351 °C. IR (KBr) ν_{max}/cm^{-1} 3440, 1760, 1708, 1673, 1648, 1611, 1505, 1488, 1370, 1332, 1299, 1269, 1176, 1070, 1042, 1012, 873, 747, 727. ^{1}H NMR (DMSO-d_6, 600 MHz) δ 11.05 (1H, s, NH), 8.10–8.08 (1H, m), 7.85–7.82 (3H, m, H-7, H-8, H-9), 7.68 (1H, t, J = 8.4 Hz), 7.61 (1H, dd, J = 9.6, 1.8 Hz), 7.40 (1H, dd, J = 8.4, 1.8 Hz), 7.24 (1H, dd, J = 7.8, 0.6 Hz), 7.20 (1H, td, J = 7.8, 1.2 Hz), 6.94 (1H, td, J = 7.8, 1.2 Hz), 6.83 (1H, d, J = 7.8 Hz), 5.04 (2H, d, J = 3.0 Hz), 5.02 (1H, dd, J = 16.2, 2.4 Hz), 4.93 (1H, d, J = 16.2 Hz). ^{13}C NMR (DMSO-d_6, 125 MHz) δ 181.3 (C-10), 179.0 (C-5), 176.7 (C-2′), 169.4 (C-1), 159.9 (1C, d, J = 248.8 Hz, C–F), 156.6, 142.0, 140.9, 135.2, 134.5, 133.7, 131.4, 130.9, 130.0, 128.8, 127.5, 126.2 (1C, d, J = 18,75 Hz, C-1″), 124.4, 122.8 (1C, d, J = 13.8 Hz), 122.6, 120.6 (1C, d, J = 8.8 Hz, C-4″), 118.6 (1C, d, J = 25 Hz, C-3″), 117.0, 108.0, 100.7, 66.4 (C-3), 47.6 (C-11), 39.83 (C-7″). HR-ESI-MS: found *m*/*z* 571.0284 and 573.0271 $[M + H]^+$ (calcd for $[C_{29}H_{17}BrFN_2O_5]^+$: 571.0300 and 573.0279) and *m*/*z* 593.0107 and 595.0093 $[M + Na]^+$ (calcd for $[C_{29}H_{16}BrFN_2NaO_5]^+$: 593.0119 and 595.0099).

5′-Chloro-1′-(4-(trifluoromethyl)benzyl)-3*H*-spiro[benzo[*g*]furo[3,4-*b*]quinoline-11,3′-indoline]-1,2′,5,10(4*H*)-tetraone (7l). Yield 490 mg (85%), red-brown solid, mp 354–355 °C. IR (KBr) ν_{max}/cm^{-1} 3442, 3303, 1762, 1705, 1670, 1595, 1503, 1485, 1431, 1323, 1301, 1268, 1160, 1121, 1067, 1042, 1014, 824, 808, 729, 695, 553. ^{1}H NMR (DMSO-d_6, 600 MHz) δ 11.10 (1H, s, NH), 8.12–8.08 (1H, m, H-6), 7.88–7.84 (3H, m, H-7, H-8, H-9), 7.84 (2H, d, J = 8.4 Hz), 7.74 (2H, d, J = 8.4 Hz), 7.38 (1H, d, J = 2.4 Hz), 7.23 (1H, dd, J = 8.4, 2.4 Hz), 6.78 (1H, d, J = 8.4 Hz), 5.14 (1H, d, J = 16.8 Hz), 5.07 (1H, d, J = 16.8 Hz), 5.06 (2H, s). ^{13}C NMR (DMSO-d_6, 125 MHz) δ 181.4 (C-10), 179.0 (C-5), 176.5 (C-2′), 169.4 (C-1), 156.9, 141.2, 141.2, 141.0, 136.1, 135.1, 133.7, 131.4, 130.1, 128.5, 128.0 (3C), 126.6, 126.2, 126.1, 125.2 (2C, d, J = 3.8 Hz), 124.7, 124.3 (1C, q, J = 270.0 Hz, CF_3), 116.4, 109.7, 100.2, 66.5 (C-3), 47.9 (C-11), 43.3 (C-7″). HR-ESI-MS: found *m*/*z* 577.0772 $[M + H]^+$ (calcd for $[C_{30}H_{17}ClF_3N_2O_5]^+$: 577.0773) and *m*/*z* 599.0593 $[M + Na]^+$ (calcd for $[C_{30}H_{17}ClF_3N_2NaO_5]^+$: 599.0593).

1′-(4-Bromo-2-fluorobenzyl)-6′-methyl-3*H*-spiro[benzo[*g*]furo[3,4-*b*]quinoline-11,3′-indoline]-1,2′,5,10(4*H*)-tetraone (7m). Yield 468 mg (80%), red-brown solid, mp (decomp.) 337–338 °C. IR (KBr) ν_{max}/cm^{-1} 3314, 2970, 1761, 1725, 1685, 1655, 1595,

1496, 1451, 1396, 1341, 1301, 1267, 1242, 1174, 1077, 1027, 875, 800, 743, 726. ^{1}H NMR (DMSO-d_6, 600 MHz) δ 11.06 (1H, s, NH), 8.09 (1H, m, H-6), 7.89–7.88 (1H, m, H-9), 7.86–7.83 (2H, m, H7, H8), 7.81 (1H, t, J = 8.4 Hz, H-6″), 7.64 (1H, dd, J = 9.6 Hz, J = 1.8 Hz, H-3″), 7.44 (1H, dd, J = 8.4 Hz, J = 1.8 Hz, H-5″), 7.09 (1H, d, J = 7.2 Hz, H-8′), 6.99 (1H, d, J = 7.2 Hz, H-5′), 6.87 (1H, t, J = 7.2 Hz, H-7′), 5.18 (1H, d, J = 17.4 Hz, H-7″), 5.13 (1H, d, J = 17.4 Hz, H-7″), 5.05 (2H, d, J = 16.8 Hz, H-3), 2.23 (3H, s, H-9). ^{13}C NMR (DMSO-d_6, 125 MHz) δ 181.3 (C-10), 178.9 (C-5), 177.8 (C-2′), 169.4 (C-1), 158.9 (1C, d, J = 247.5 Hz, C–F), 156.4 (C-3a), 140.8 (C-4a), 139.98 (C-4′), 135.5 (C-6′), 135.1 (C-8), 133.7 (C-7), 132.5 (C-5′), 131.4 (C-9a), 129.98 (C-5a), 129.8 (1C, d, J = 4.5 Hz, C-6″), 127.8 (C-5″), 126.2 (C-6), 126.1 (C-9), 125.2 (1C, d, J = 15.0 Hz, C-1″), 122.6 (C-7′, C-8′), 120.4 (1C, d, J = 9.0 Hz, C-4″), 118.6 (1C, d, J = 24 Hz, C-3″), 118.3 (C-3′), 117.3 (C-10a), 100.9 (C-11a), 66.4 (C-3), 47.1 (C-11), 39.92 (C-7″), 17.3 (C-9′). HR-ESI-MS: found m/z 585.04564 and 587.0436 $[M + H]^+$ (calcd for $[C_{30}H_{19}BrFN_2O_5]^+$: 585.0456 and 587.0436) and m/z 607.0273 and 609.0256 $[M + Na]^+$ (calcd for $[C_{30}H_{18}BrFN_2NaO_5]^+$: 607.0276 and 609.0255).

5′,6′-Dibromo-1′-(4-(trifluoromethyl)benzyl)-3*H*-spiro[benzo[*g*]furo[3,4-*b*]quinoline-11,3′-indoline]-1,2′,5,10(4*H*)-tetraone (7n). Yield 504 mg (72%), orange-red solid, mp 278–279 °C. IR (KBr) ν_{max}/cm^{-1} 3431, 3067, 2957, 2926, 1751, 1728, 1668, 1645, 1596, 1501, 1456, 1397, 1324, 1267, 1161, 1127, 1067, 1039, 1023, 1010, 974, 804, 739, 727, 551. ^{1}H NMR (DMSO-d_6, 600 MHz) δ 11.19 (1H, s, NH), 8.11 (1H, dd, J = 6.6, 2.4 Hz, H-6), 7.93 (1H, dd, J = 6.6, 2.4 Hz, H-9), 7.89–7.85 (2H, m, H-7, H-8), 7.79 (2H, d, J = 8.4 Hz, H-3″, H-5″), 7.73 (2H, d, J = 8.4 Hz, H-2″, H-6″), 7.63 (1H, d, J = 2.4 Hz, H-8′), 7.59 (1H, d, J = 2.4 Hz, H-5′), 5.42 (2H, s), 5.08 (2H, s). ^{13}C NMR (DMSO-d_6, 125 MHz) δ 181.6 (C-10), 178.8 (C-5), 177.4 (C-2′), 169.5 (C-1), 157.1, 143.0, 141.4, 139.3, 139.2, 135.5, 135.2, 133.9, 131.3, 130.2, 127.2, 127.0 (2C), 126.3, 126.2, 125.2 (2C, d, J = 3.8 Hz), 124.3 (1C, q, J = 270.0 Hz, CF_3), 116.1, 115.1, 101.6, 100.0, 66.7 (C-3), 47.7 (C-11), 44.9 (C-7″). HR-ESI-MS: found m/z 700.9359 and 698.9366 and 702.9299 $[M + H]^+$ (calcd for $[C_{30}H_{16}Br_2F_3N_2O_5]^+$: 700.9353 and 698.9373 and 702.9332).

Cell culture and cell viability assay

Epidermoid carcinoma (KB, ATCC number CCL-17), hepatocellular carcinoma (HepG2, ATCC number HB-8065), lung (A549) cancer, breast (MCF7, HTB-22™) cancer cell lines, and human embryonic kidney (HEK-293, ATCC number CRL-1573) cell line were sourced from the American Type Culture Collection (ATCC, USA). The cells were cultured in DMEM (Dulbecco's Modified Eagle Medium) medium, supplemented with 10% fetal bovine serum, 100 U per mL penicillin, and 100 μg per mL streptomycin, under a humidified atmosphere (95% air and 5% CO_2) at 37 °C. The exponentially growing cells were used throughout the experiments. Cytotoxic effects of products **7a–n** on the growth of human cancer cells were evaluated using MTT (3-(4,5-dimethylthiazol-2-yl)-2,5-diphenyltetrazolium bromide) assay. Human cancer cell lines (3×10^4 cells per mL) were treated with solutions of products **7** in DMSO. After incubating for 3 days, 10 μL solution of 5 mg mL^{-1} MTT in sodium phosphate buffer (PBS, 0.1 M, pH 7.4) was added to each well, and the cells were incubated at 37 °C for 4 hours. The medium was then carefully removed, and DMSO (150 μL) was added to each well to dissolve the obtained formazan crystals. Absorbance of the solutions was measured at a 540 nm wavelength with a Biotek Epoch 2 microplate reader. Percentage of growth inhibition was determined by comparing the absorbance of treated samples to that of control samples without the compounds. A dose–response curve was generated, and the IC_{50} values for each compound against both cell lines were determined.[32,41]

Cell cycle analysis

A549 cancer cells were seeded in 25 cm^2 flasks (Corning, USA) at a density of 3×10^5 cells and treated with different concentrations of product **7f** at 0.45 μM, 0.9 μM and 1.8 μM or DMSO 0.5% (negative reference) for 24 hours. After treatment, the cells were harvested and washed twice with phosphate-buffered saline (PBS). They were then fixed with ice-cold ethanol 70% at −20 °C for 2 hours, followed by low-speed centrifugation at 2000 rpm for 5 minutes to collect the cells. After washing, the cells were resuspended in 0.45 mL PBS and incubated with RNase A (2.5 mg mL^{-1}) at 37 °C for 15 minutes. Next, the cells were stained with 2.5 μL propidium iodide (PI) (1 mg mL^{-1}) for 30 minutes and diluted with 500 μL PBS. The samples were analyzed by a flow cytometry (Novocyte, ACEA Biosciences, San Diego, CA, USA) and data were analyzed and reported by ACEA's NovoExpress software.[32,41]

Annexin-V FITC and PI flow cytometry assay for apoptosis

The extent of apoptosis was quantitatively measured using the kit annexin V and PI/dead cell apoptosis® from Invitrogen. Briefly, A549 cancer cells were seeded in 25 cm^2 flasks (Corning, USA) at a density of 5×10^5 cells and treated with different concentrations of product **7f** (0.45 μM, 0.9 μM and 1.8 μM) or DMSO 1% and camptothecin (2 μM) for 48 h. Then, the cells were collected into falcon tubes, centrifuged, and washed with cold PBS. The washed cells were re-centrifuged, and the supernatant was discarded. Then, the cells were resuspended in 100 μL of binding buffer and stained with 5 μL of annexin V and 1 μL of propidium iodide (PI) (1 mg mL^{-1}). The cells were incubated for 15 minutes at 37 °C, after which 400 μL of binding buffer was added. The samples were analyzed by a Novocyte flow cytometry system, and data were analyzed and reported by NoVo Express software (ACEA Bioscience Inc.).[32,41]

Molecular docking study

Molecular docking simulations were performed to evaluate the binding ability of compound **7f** against common cytotoxic targets according to our chemical design. ICM-pro 3.8.3 (Molsoft, L.L.C.) was employed for this purpose, taking into consideration the previous configurations.[30,31,57,58] Three proteins with crystalized three-dimensional (3D) structures in the Protein Data Bank were selected, including two human cyclin-dependent kinase (CDK) complexes, CDK2/cyclin A in complex with ATP (PDB ID 1FIN) and CDK5/p25 in complex with

(*R*)-roscovitine (PDB ID 1UNL), and procaspase locked by Zn ion (PDB ID 4FXO).[45,46,48] The 3D structure of compound **7f** was created by ChemAxon Marvin Suite version 22.5 and optimized using the force field MMFF94s through the steepest-descent method with a convergence criterion of 1×10^{-5}. Receptor preparation was carried out following the previous reports which include consecutive steps such as correction of protonation states, active site identification using ICM Pocket Finder, occupancy and *b*-factor check, optimization of polar hydrogen atoms, setup of rotameric states for His–Pro–Gly–Cys residues, and ICMFF force field for global system. The docking simulations were then performed, generating 10^3 conformations. The top-scoring poses were ranked and analyzed based on the GBSA/MM-type scoring function, whose features include the conventional interactions and internal force field energy, *e.g.*, hydrophobic van der Waals, electrostatic interaction, solvation/desolvation, conformational loss energy and hydrogen bonding.

Prediction of physicochemical and ADMET (absorption, distribution, metabolism, excretion, and toxicity) properties

Significant physicochemical properties related to ADMET processes were computed using ADMETlab 3.0 web server (**https://admetlab3.scbdd.com/**) and other tools.[51–54] The properties related to the Biopharmaceutics Classification System (BCS) of drugs, including aqueous solubility, epithelial permeability, human intestinal absorption, and metabolism extent, were computed.[52] In addition, drug-like indices were calculated based on rule-of-thumb methods,[51,54,55] including Lipinski, Prizer, SGK, 3PRule, *etc.* In total, 120 pharmacokinetic and toxicity properties were computed and discussed in accordance with the current standard for preclinical screening of drug candidates.

Conclusions

In summary, the effective synthesis of isatin–podophyllotoxin derivatives **7a–n** through a microwave-facilitated three-component reaction of 2-amino-1,4-naphthoquinone, tetronic acid, and substituted isatin derivatives in glacial acetic acid in the presence of *p*-toluenesulfonic acid as a catalyst has been described. Cytotoxic effects of products were evaluated using 3-(4,5-dimethylthiazol-2-yl)-2,5-diphenyltetrazolium bromide (MTT) assay. All products **7a–n** displayed moderate to strong inhibitory activity against four cancer cell lines, with IC_{50} values ranging from 0.90 to 51.68 μM, indicating the potential of these compounds for the treatment of cancer. Among the products, product **7f** displayed the most potent cytotoxicity, with IC_{50} values of 1.99 ± 0.22 and 0.90 ± 0.09 μM against KB and A549 cell lines, respectively. In addition, product **7f** could arrest the cell cycle of A549 cells at S phase and trigger apoptosis in a dose-dependent manner. Molecular docking simulation of product **7f** revealed the expected binding mode which involves the accommodation of product **7f** at the ATP binding sites of CDK2/cyclin A and CDK5/p25 as well as stable bidentate chelation of **7f** with the inhibitory Zn ion. Based on the docking results, this compound was found to have antiproliferative activity against cancer cells by inhibiting activation of CDK2/cyclin A complex as well as anti-tumorigenesis by targeting CDK5/p25 complex. In addition, **7f** was estimated to induce the apoptosis process by sequestering Zn bound to procaspase in the same manner as PAC-1, a procaspase activator that induces G1/S cell cycle arrest and blocks DNA synthesis in cancer cells. These findings are in agreement with the previous reports relating to the anticancer mechanism of podophyllotoxin derivatives. Physicochemical and ADMET calculations for **7f** revealed that first-pass metabolism and liver toxicity would be significant issues to be addressed in the next hit-to-lead optimization. Otherwise, it accomplished almost all the drug-like rule and preclinical safety requirements in the anticancer drug discovery process.

Data availability

The datasets supporting this article have been uploaded as part of the ESI.†

Author contributions

Ha Thanh Nguyen: investigation: synthesis and characterizations of compounds; writing – original draft. Ket Tran Van: investigation: synthesis and characterizations of compounds. Hai Pham-The and Bao Le-Quang: investigation: molecular docking and computational studies. Giang Le-Nhat-Thuy and Tuyet Anh Dang Thi: investigation: biological activity evaluation of potent compounds. Phuong Hoang Thi and Quynh Giang Nguyen Thi: investigation: characterizations of compounds. Tuan Anh Nguyen and Doan Vu Ngoc: investigation: revised draft. Tuyen Van Nguyen: project administration; supervision: conceptual design; writing – review & editing.

Conflicts of interest

There are no conflicts to declare.

Acknowledgements

This work was supported by National Foundation for Science and Technology Development (NAFOSTED) [grant number: 104.01-2023.19].

Notes and references

1 M. B. Parmar, M. K. Vara and J. H. Pandya, A brief review on imidazole, triazine, and isatin derivatives: synthesis approaches and their applications, *Discover Chemistry*, 2024, **1**, 56.
2 A. E. Medvedev, A. Clow, M. Sandler and V. Glover, Isatin: a link between natriuretic peptides and monoamines?, *Biochem. Pharmacol.*, 1996, **52**, 385–391.
3 A. E. Medvedev and V. Glover, Tribulin and endogenous mao-inhibitory regulation in vivo, *Neurotoxicology*, 2004, **25**, 185–192.

4 A. Medvedev, N. Igosheva, M. Crumeyrolle-Arias and V. Glover, Isatin: role in stress and anxiety, *Stress*, 2005, **8**, 175–183.
5 T. E. Malah, H. Farag, B. A. Hemdan, R. E. A. Mageid, M. T. Abdelrahman, M. A. El-Manawaty and H. F. Nour, Synthesis, in vitro antimicrobial evaluation, and molecular docking studies of new isatin-1,2,3-triazole hybrids, *J. Mol. Struct.*, 2022, **1250**, 131855.
6 C. S. Marques, A. González-Bakker, J. M. Padrón and A. J. Burke, Easy access to Ugi-derived isatin-peptoids and their potential as small-molecule anticancer agents, *New J. Chem.*, 2023, **47**, 743–750.
7 R. S. Cheke, V. M. Patil, S. D. Firke, J. P. Ambhore, I. A. Ansari, H. M. Patel, S. D. Shinde, V. R. Pasupuleti, M. I. Hassan, M. Adnan, A. Kadri and M. Snoussi, Therapeutic outcomes of isatin and its derivatives against multiple diseases: recent developments in drug discovery, *Pharmaceuticals*, 2022, **15**, 272.
8 K. Lahari and R. Sundararajan, Design and synthesis of novel isatin derivatives as potent analgesic, anti-inflammatory and antimicrobial agents, *J. Chem. Sci.*, 2020, **132**, 94.
9 T. K. Bakır, M. S. Çavuş, H. Muğlu and H. Yakan, Synthesis, structure elucidation, antioxidant properties, and theoretical calculations of new Schiff bases–isatin derivatives, *Res. Chem. Intermed.*, 2024, **50**, 3937–3962.
10 V. Varun, S. Sonam and R. Kakkar, Isatin and its derivatives: a survey of recent syntheses, reactions, and applications, *Med. Chem. Commun.*, 2019, **10**, 351–368.
11 H. M. Alkahtani, M. M. Alanazi, F. S. Aleanizy, F. Y. Alqahtani, A. Alhoshani, F. E. Alanazi, A. A. Almehizia, A. N. Abdalla, M. G. Alanazi, A. S. El-Azab and A. A.-M. Abdel-Aziz, Synthesis, anticancer, apoptosis-inducing activities and EGFR and VEGFR2 assay mechanistic studies of 5,5-diphenylimidazolidine-2,4-dione derivatives: molecular docking studies, *Saudi Pharm. J.*, 2019, **27**, 682–693.
12 A. S. Alanazi, T. O. Mirgany, A. A. Alsfouk, N. A. Alsaif and M. M. Alanazi, Antiproliferative activity, multikinase inhibition, apoptosis inducing effects and molecular docking of novel isatin–purine hybrids, *Medicina*, 2023, **59**, 610.
13 Z. Li, J. Ma, M. Tian, P. Xia, X. Lv, R. Hou, Y. Jiang, X. Xu, Z. Jia, J. Wang and Z. Li, Synthesis, biological activity evaluation and mechanism of action of novel bis-isatin derivatives as potential anti-liver cancer agents, *Bioorg. Med. Chem. Lett.*, 2024, **99**, 129613.
14 M. Altamimi, S. A. Syed, B. Tuzun, M. R. Alhazani, O. Alnemer and A. Bari, Synthesis, biological evaluation and molecular docking of isatin hybrids as anti-cancer and anti-microbial agents, *J. Enzyme Inhib. Med. Chem.*, 2024, **39**, 2288548.
15 A. Mushtaq, R. Asif, W. A. Humayun and M. M. Naseer, Novel isatin–triazole based thiosemicarbazones as potential anticancer agents: synthesis, DFT and molecular docking studies, *RSC Adv.*, 2024, **14**, 14051–14067.
16 G. Kumar, N. P. Singh and K. Kumar, Recent advancement of synthesis of isatins as a versatile pharmacophore: a review, *Drug Res.*, 2021, **71**, 115–121.
17 Preeti, A. Raza, A. Anand, N. Henry, A. K. Sharma, P. Roussel and V. Kumar, Stereo/regio-selective access to substituted 3-hydroxy-oxindoles with anti-proliferative assessment and in silico validation, *RSC Adv.*, 2023, **13**, 28434–28443.
18 A. Andreani, M. Granaiola, A. Leoni, A. Locatelli, R. Morigi, M. Rambaldi, V. Garaliene, W. Welsh, S. Arora, G. Farruggia and L. Masotti, antitumor activity of new substituted 3-(5-imidazo[2,1-*b*]thiazolylmethylene)-2-indolinones and study of their effect on the cell cycle, *J. Med. Chem.*, 2005, **48**, 5604–5607.
19 R. E. Ferraz De Paiva, E. G. Vieira, D. Rodrigues Da Silva, C. A. Wegermann and A. M. C. Ferreira, Anticancer compounds based on isatin-derivatives: strategies to ameliorate selectivity and efficiency, *Front. Mol. Biosci.*, 2021, **7**, 627272.
20 A. K. Gupta, S. Tulsyan, M. Bharadwaj and R. Mehrotra, systematic review on cytotoxic and anticancer potential of N-substituted isatins as novel class of compounds useful in multidrug-resistant cancer therapy: in silico and in vitro analysis, *Top. Curr. Chem.*, 2019, **377**, 15.
21 M. Gordaliza, P. A. García, J. M. Miguel del Corral, M. A. Castro and M. A. Gómez-Zurita, Podophyllotoxin: distribution, sources, applications and new cytotoxic derivatives, *Toxicon*, 2004, **44**, 441–459.
22 H. Ardalani, A. Avan and M. Ghayour-Mobarhan, Podophyllotoxin: a novel potential natural anticancer agent, *Avicenna J. Phytomed.*, 2017, **7**, 10.
23 N. H. Thanh, L. Q. Bao, H. Pham-The, D. T. T. Anh and P. V. Kiem, Synthesis, molecular docking, and cytotoxic evaluation of fluorinated podophyllotoxin derivatives, *Nat. Prod. Commun.*, 2023, **18**(2), 1–7.
24 N. Jeedimalla, M. Flint, L. Smith, A. Haces, D. Minond and S. P. Roche, Multicomponent assembly of 4-aza-podophyllotoxins: a fast entry to highly selective and potent anti-leukemic agents, *Eur. J. Med. Chem.*, 2015, **106**, 167–179.
25 N. H. Thanh, H. T. Phuong, L. T. T. Anh, L. N. T. Giang, N. T. Q. Giang, N. T. Anh, D. T. T. Anh and P. V. Kiem, Synthesis and cytotoxic evaluation of fluoro and trifluoromethyl substituents containing novel naphthoquinone-fused podophyllotoxins, *Nat. Prod. Commun.*, 2022, **17**(10), 1–6.
26 H. T. Nguyen, G. Le-Nhat-Thuy, P. H. Thi, Q. G. N. Thi, T. A. Nguyen, T. H. N. Thi, T. A. D. Thi and T. V. Nguyen, Microwave-assisted three-component synthesis of novel *n*-arylated-dihydrobenzo[*g*]quinoline-5,10-diones and their potential cytotoxic activity, *Chem. Biodiversity*, 2022, **19**, e202200359.
27 Y. Hitotsuyanagi, M. Fukuyo, K. Tsuda, M. Kobayashi, A. Ozeki, H. Itokawa and K. Takeya, 4-Aza-2,3-dehydro-4-deoxypodophyllotoxins: simple aza-podophyllotoxin analogues possessing potent cytotoxicity, *Bioorg. Med. Chem. Lett.*, 2000, **10**, 315–317.

28 H. Naeimi, Z. Rashid, A. H. Zarnani and R. Ghahremanzadeh, An Efficient one-pot multicomponent synthesis of 4-aza-podophyllotoxin derivatives in ionic liquid, *J. Chem.*, 2013, **2013**, 1–9.

29 X. Yang, C. Zhang and L. Wu, l -Proline catalyzed three-component synthesis of para-naphthoquinone–4-aza-podophyllotoxin hybrids as potent antitumor agents, *RSC Adv.*, 2015, **5**, 18945–18951.

30 H. T. Nguyen, K. T. Van, H. Pham-The, J. Braire, P. H. Thi, T. A. Nguyen, Q. G. N. Thi, T. A. D. Thi, G. Le-Nhat-Thuy, T. A. L. Thi, D. V. Ngoc and T. N. Van, Synthesis, molecular docking analysis and in vitro evaluation of new heterocyclic hybrids of 4-aza-podophyllotoxin as potent cytotoxic agents, *RSC Adv.*, 2024, **14**, 1838–1853.

31 H. T. Nguyen, Q. G. N. Thi, T. H. N. Thi, P. H. Thi, G. Le-Nhat-Thuy, T. A. D. Thi, B. Le-Quang, H. Pham-The and T. V. Nguyen, Synthesis and biological activity, and molecular modelling studies of potent cytotoxic podophyllotoxin-naphthoquinone compounds, *RSC Adv.*, 2022, **12**, 22004–22019.

32 Q. G. N. Thi, G. Le-Nhat-Thuy, T. A. D. Thi, P. H. Thi, A. N. Tuan, T. H. N. Thi, T. T. Nguyen, T. N. Ha, H. H. Mai and T. V. Nguyen, Synthesis of novel potent cytotoxicy podophyllotoxin-naphthoquinone compounds via microwave-assisted multicomponent domino reactions, *Bioorg. Med. Chem. Lett.*, 2021, **37**, 127841.

33 T. S. Morais, Recent advances in the development of hybrid drugs, *Pharmaceutics*, 2024, **16**(7), 889.

34 M. Dabiri, Z. N. Tisseh, M. Bahramnejad and A. Bazgir, Sonochemical multi-component synthesis of spirooxindoles, *Ultrason. Sonochem.*, 2011, **18**, 1153–1159.

35 H. T. Nguyen, H. Pham-The, A. N. Tuan, H. N. T. Thu, T. A. D. Thi, G. Le-Nhat-Thuy, P. H. Thi, Q. G. N. Thi and T. V. Nguyen, Improved synthesis, molecular modeling and anti-inflammatory activity of new fluorinated dihydrofurano-naphthoquinone compounds, *Bioorg. Med. Chem. Lett.*, 2024, **104**, 129714.

36 G. Le-Nhat-Thuy, T. A. D. Thi, P. H. Thi, Q. G. N. Thi, H.-T. Nguyen, D. V. Ngoc, T.-A. Nguyen and T. V. Nguyen, Multicomponent synthesis of novel 3-benzoyl-4h-benzo[g] chromene-5,10-dione derivatives, *Tetrahedron Lett.*, 2021, **75**, 153215.

37 H. T. Nguyen, T. H. N. Thi, J. Braire, T. A. D. Thi and T. N. Van, Microwave-assisted multicomponent synthesis of new 6-arylated 5-hydroxy-benzo[*a*]phenazine derivatives and their potential anti-inflammatory activity, *ChemistrySelect*, 2023, **8**, e202204376.

38 H. T. Nguyen, A. N. Tuan, T. A. D. Thi, K. T. Van, G. Le-Nhat-Thuy, P. H. Thi, Q. G. N. Thi, C. B. Thi, H. T. Quang and T. V. Nguyen, Synthesis, in vitro A-glucosidase, and acetylcholinesterase inhibitory activities of novel indol-fused pyrano[2,3-*D*]pyrimidine compounds, *Bioorg. Med. Chem. Lett.*, 2024, **98**, 129566.

39 H. T. Nguyen, H. N. Van, P. H. Thi, T. A. D. Thi, G. Le-Nhat-Thuy, Q. G. N. Thi, A. N. Tuan, C. B. Thi, H. T. Quang and T. V. Nguyen, Synthesis and cytotoxic evaluation of new fluoro and trifluoromethyl substituents containing chromeno[2,3- *d*]pyrimidines, *ChemistrySelect*, 2023, **8**, e202300227.

40 N. H. Thanh, N. T. Q. Giang, N. V. Ha, H. T. Phuong, L. N. T. Giang, N. T. Anh, B. T. Cham, L. D. Huy, D. T. T. Anh, P. V. Kiem and N. V. Tuyen, Synthesis and evaluation of acetylcholinesterase inhibitory and cytotoxic activities of pyrano[2,3- *d*]pyrimidines, *Nat. Prod. Commun.*, 2023, **18**(9), 1–10.

41 N. H. Thanh, N. T. T. Ha, N. T. Tra, L. T. T. Anh, N. T. Son, N. V. Tuyen and P. V. Kiem, Bannaxanthone E induced cell-cycle arrest and apoptosis in human lung cancer cell line, *Nat. Prod. Commun.*, 2021, **16**(11), 1–6.

42 V. A. Fadok, D. L. Bratton, S. C. Frasch, M. L. Warner and P. M. Henson, The role of phosphatidylserine in recognition of apoptotic cells by phagocytes, *Cell Death Differ.*, 1998, **5**, 551–562.

43 H. A. Andree, C. P. Reutelingsperger, R. Hauptmann, H. C. Hemker, W. T. Hermens and G. M. Willems, Binding of vascular anticoagulant alpha (VAC alpha) to planar phospholipid bilayers, *J. Biol. Chem.*, 1990, **265**, 4923–4928.

44 S. L. Rath and S. Senapati, Molecular basis of differential selectivity of cyclobutyl-substituted imidazole inhibitors against cdks: insights for rational drug design, *PLoS One*, 2013, **8**, e73836.

45 P. D. Jeffrey, A. A. Russo, K. Polyak, E. Gibbs, J. Hurwitz, J. Massagué and N. P. Pavletich, Mechanism of CDK activation revealed by the structure of a cyclinA-CDK2 complex, *Nature*, 1995, **376**, 313–320.

46 M. Mapelli, L. Massimiliano, C. Crovace, M. A. Seeliger, L.-H. Tsai, L. Meijer and A. Musacchio, Mechanism of cdk5/p25 binding by cdk inhibitors, *J. Med. Chem.*, 2005, **48**, 671–679.

47 M. D. Vivo, G. Bottegoni, A. Berteotti, M. Recanatini, F. L. Gervasio and A. Cavalli, Cyclin-dependent kinases: bridging their structure and function through computations, *Future Med. Chem.*, 2011, **3**, 1551–1559.

48 E. M. Velázquez-Delgado and J. A. Hardy, Zinc-mediated allosteric inhibition of caspase-6, *J. Biol. Chem.*, 2012, **287**, 36000–36011.

49 D. T. M. Dung, E. J. Park, D. T. Anh, P.-T. Hai, L. Q. Bao, A. Y. Ji, J. S. Kang, T. T. Tung, S.-B. Han and N.-H. Nam, Design, synthesis and evaluation of novel (E)-N'-((1-(4-chlorobenzyl)-1H-indol-3- yl)methylene)-2-(4-oxoquinazolin-3(4H)-yl)acetohydrazides as antitumor agents, *Anti-Cancer Agents Med. Chem.*, 2022, **22**, 2586–2598.

50 L. C. Huan, D. T. Anh, B. X. Truong, P. H. Duc, P.-T. Hai, L. Duc-Anh, L.-T.-T. Huong, E. J. Park, H. J. Lee, J. S. Kang, P.-T. Tran, D. T. T. Hai, D. T. K. Oanh, S.-B. Han and N.-H. Nam, New acetohydrazides incorporating 2-oxoindoline and 4-oxoquinazoline: synthesis and evaluation of cytotoxicity and caspase activation activity, *Chem. Biodiversity*, 2020, **17**, e1900670.

51 L. Fu, S. Shi, J. Yi, N. Wang, Y. He, Z. Wu, J. Peng, Y. Deng, W. Wang, C. Wu, A. Lyu, X. Zeng, W. Zhao, T. Hou and D. Cao, ADMETlab 3.0: an updated comprehensive online ADMET prediction platform enhanced with broader

coverage, improved performance, API functionality and decision support, *Nucleic Acids Res.*, 2024, **52**, W422–W431.

52 H. Pham-The, T. Garrigues, M. Bermejo, I. González-Álvarez, M. C. Monteagudo and M. Á. Cabrera-Pérez, Provisional classification and in silico study of biopharmaceutical system based on caco-2 cell permeability and dose number, *Mol. Pharmaceutics*, 2013, **10**, 2445–2461.

53 J. A. Castillo-Garit, G. M. Casanola-Martin, H. Le-Thi-Thu, H. Pham-The and S. J. Barigye, A simple method to predict blood-brain barrier permeability of drug- like compounds using classification trees, *Med. Chem.*, 2017, **13**, 664–669.

54 H. Pham-The, I. González-Álvarez, M. Bermejo, T. Garrigues, H. Le-Thi-Thu and M. Á. Cabrera-Pérez, The use of rule-based and qspr approaches in AMDE profiling: a case study on caco-2 permeability, *Mol. Inf.*, 2013, **32**, 459–479.

55 H. Pham-The, M. Á. Cabrera-Pérez, N.-H. Nam, J. A. Castillo-Garit, B. Rasulev, H. Le-Thi-Thu and G. M. Casañola-Martin, In silico assessment of ADME properties: advances in caco-2 cell monolayer permeability modeling, *Curr. Top. Med. Chem.*, 2019, **18**, 2209–2229.

56 Y. Perez-Castillo, A. Sánchez-Rodríguez, E. Tejera, M. Cruz-Monteagudo, F. Borges, M. N. D. S. Cordeiro, H. Le-Thi-Thu and H. Pham-The, A desirability-based multi objective approach for the virtual screening discovery of broad-spectrum anti-gastric cancer agents, *PLoS One*, 2018, **13**, e0192176.

57 L. C. Huan, C. V. Phuong, L. C. Truc, V. N. Thanh, H. Pham-The, L.-T.-T. Huong, N. T. Thuan, E. J. Park, A. Y. Ji, J. S. Kang, S.-B. Han, P.-T. Tran and N.-H. Nam, (*E*)- *N'* -Arylidene-2-(4-oxoquinazolin-4(3 *H*)-yl) acetohydrazides: Synthesis and evaluation of antitumor cytotoxicity and caspase activation activity, *J. Enzyme Inhib. Med. Chem.*, 2019, **34**, 465–478.

58 M. A. C. Neves, M. Totrov and R. Abagyan, Docking and scoring with ICM: the benchmarking results and strategies for improvement, *J. Comput.-Aided Mol. Des.*, 2012, **26**, 675–686.